Volume coil based on hybridized resonators for magnetic resonance imaging

C. Jouvaud, Redha Abdeddaim, B. Larrat, Julien de Rosny

Volume coil based on hybridized resonators for magnetic resonance imaging

C. Jouvaud, R. Abdeddaim, B. Larrat, and J. de Rosny

Citation: Appl. Phys. Lett. **108**, 023503 (2016);
View online: https://doi.org/10.1063/1.4939784
View Table of Contents: http://aip.scitation.org/toc/apl/108/2
Published by the American Institute of Physics

Volume coil based on hybridized resonators for magnetic resonance imaging

C. Jouvaud,[1,2] R. Abdeddaim,[1,3] B. Larrat,[1] and J. de Rosny[1]
[1]*ESPCI ParisTech, CNRS, PSL Research University, Institut Langevin, 1 rue Jussieu, F-75005 Paris, France*
[2]*CEA, DAM, GRAMAT, F-46500 Gramat, France*
[3]*Aix-Marseille Université, CNRS, Centrale Marseille, Institut Fresnel, UMR 7249, Avenue Escadrille Normandie-Niemen, 13397 Marseille Cedex, France*

(Received 9 November 2015; accepted 30 December 2015; published online 12 January 2016)

We present an electromagnetic device based on hybridization of four half-wavelength dipoles which increases the uniformity and the strength of the radio-frequency (RF) field of a Magnetic Resonant Imaging (MRI) apparatus. Numerical results show that this Hybridized Coil (HC) excited with a classical loop coil takes advantage of the magnetic hybrid modes. The distribution of the RF magnetic field is experimentally confirmed on a 7-T MRI with a gelatin phantom. Finally, the HC is validated *in vivo* by imaging the head of an anesthetized rat. We measure an overall increase of the signal to noise ratio with up to 2.4 fold increase in regions of interest far from the active loop coil. © *2016 AIP Publishing LLC*. [http://dx.doi.org/10.1063/1.4939784]

Imaging objects and bodies with non-invasive techniques is a challenging field in physics. In this area, Magnetic Resonance Imaging (MRI) is one of the major diagnostic modalities based on the quantum spin of nuclei.[1] Under a static magnetic field $B0$, spins tend to align either positively or negatively, giving rise to a positive net magnetization along $B0$. At equilibrium, this magnetization is constant and aligned with $B0$. When spins are excited by a transient transverse radio-frequency (RF) magnetic field B1, generated by a coil at the Larmor frequency, they start to precess around B0 at this resonance frequency. Precession occurs at the Larmor frequency inherent to each atom's nucleus. Transitions occur between the up and down spin states and spins start to precess, all in phase, giving rise to a net magnetization in the plane transverse to B0. At the end of the emission, the nuclei spins relax and emit a decaying RF magnetic field at the Larmor frequency. The image is constructed following spatial encoding of the radiofrequency signals by the transient application of magnetic field gradients. The quality of an image defined by many interdependent variables (pixel size, contrast, signal to noise ratio (SNR), and homogeneity) is driven by all IRM parameters: sequence, gradients, and geometry. The transmit and receive RF apparatus impact the signal to noise ratio and the homogeneity of the image, because they mainly govern the B1 field strength and distribution. Two main types of coils have been proposed to emit and receive the B1 field: the surface coils showing strong SNR but bad homogeneity (Helmholtz loop coil and multi-slot surface coil[2]) and volume coils which generate a more uniform B1 field but do so at the expense of a smaller SNR (Helmholtz Pair Coil and Bird Cage Coil[3]). In recent decades, research has driven into ever increasing field strengths in order to increase both SNR and contrast to noise ratio and therefore to reach better resolution and/or reduce acquisition times. However, a higher magnetic field translates into higher Larmor frequencies, i.e., smaller wavelengths of RF field, which in turn yields some disadvantageous consequences. This includes an inhomogeneous pattern of B1 field which results in inhomogeneous pattern of flip angles on spins, reduced penetration due to strong attenuations, and specific absorption rate (SAR) increase. To overcome such consequences, the RF antenna handling the field has to be adapted. An elegant, though costly and complex solution, is the use of multiple receive[4] and multiple transmit antenna arrays.[5] The use of a tailored RF pulse allows to counterbalance the flip angle inhomogeneities while keeping SAR below regulatory limits during transmission.[6] Combining signals received from coil arrays allows the maintenance of optimal sensitivity with good homogeneity within the imaging volume. Another approach suggests to work on the B1 field of a single individual coil, in order to make that field stronger and more homogeneous with a complex arrangement of resonators.[7–11]

In this study, we propose a new volume coil based on the hybridization of resonators[12] that offers a good tradeoff between field homogeneity and SNR. We first describe how hybridization between 4 resonators yields two modes that mainly interact with the B1 field, generated by a single loop coil. We propose a simple electrodynamic model to describe the hybridization. Numerical simulations are performed using CST Microwaves Studio to survey the effect of coupling between the excitation coil and the hybridized coil (HC). This HC is validated experimentally and numerically on a phantom made of gelatin. Finally, we show how HC enhances the image quality of a rat head compared to a loop coil.

A structure composed of several resonators presents different eigenmodes. This is due to the strong near field coupling between the resonators. Fundamental modes of the individual resonators are then hybridized. To build our magnetic coil, we apply this effect to electric dipole resonators. First, let us consider a resonator which mainly interacts with the electric field and shows a fundamental mode at the angular frequency ω_0 (see Fig. 1). When two such resonators are close enough, the fundamental mode of the two resonators is split into two modes that resonate at two different frequencies ω^+ and ω^-. Due to mirror symmetry, one of the eigenmodes is symmetric, while the other one is antisymmetric. Contrary to the symmetric mode, the currents in the resonators of the antisymmetric mode are opposite in direction. Consequently, this mode can be regarded as magnetic. In our case, this antisymmetric mode is found at a lower frequency

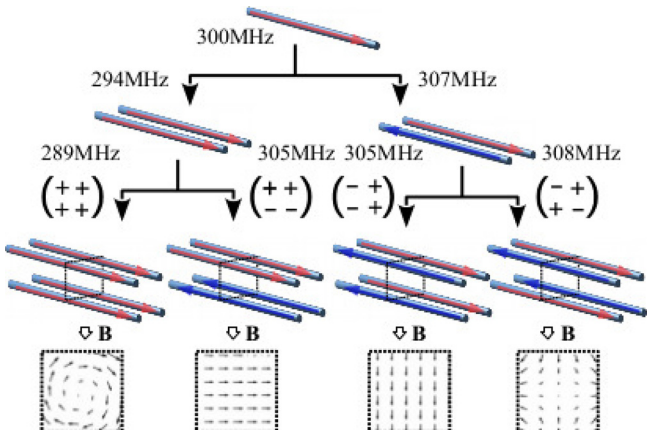

FIG. 1. Hybridization scheme of coupled half-wavelength resonators in free space. The resonators are 375 mm long and their diameter equals 1 mm. The closest resonators are 35 mm apart from each other. The red and blue arrows show the direction of the currents inside the wires. The magnetic vector field generated by each mode is shown inside the dotted squares.

than ω_0. The sub-radiant nature of this hybridized mode results in a narrow spectral bandwidth. Fig. 1 presents the 4 modes splitting from the hybridization of a pair of two-level hybridized resonators.

One way to estimate the eigen-frequencies of the structure is to compute the self and mutual impedances between the 4 resonators Z_{ij}, where i and j stand for the resonator index. For thin half wavelength resonators, a good approximation is to consider a sinusoidal distribution of the current on each resonators. Because of this assumption, Z_{ij} can be estimated from a simple numerical integration.[13] From the 4×4 elements Z_{ij}, the impedance matrix is built. The 4 modes of the structure correspond to the 4 eigen-vectors $\mathbf{I}_\alpha$ of $\mathbf{Z}$. Because of the two mirror symmetries, components of $\mathbf{I}^\alpha$ are either in phase or out of phase. For this reason, the 4 modes are written $\left(\begin{smallmatrix}-&+\\+&-\end{smallmatrix}\right)$, $\left(\begin{smallmatrix}-&+\\-&+\end{smallmatrix}\right)$, $\left(\begin{smallmatrix}-&+\\+&-\end{smallmatrix}\right)$, and $\left(\begin{smallmatrix}+&+\\+&+\end{smallmatrix}\right)$, and they are shown in Fig. 1. A similar approach has been applied in Ref. 14. Assuming the distance between the wires is shorter than their length, the magnetic field is well approximated by

$$\mathbf{B}^\alpha(\mathbf{r}) = \frac{-jk_0\mu_0}{4}\sum_{i=1}^{4} I_i^\alpha H_1^{(2)}(k_0\|\mathbf{r}-\mathbf{r}_i\|)\mathbf{u}_i^\theta, \qquad (1)$$

where $H_1^{(2)}$ is the Henkel function of second kind and first order, $\mathbf{r}_i$ is the center position of the i-th resonator, $\mathbf{u}_i^\theta$ is the tangential unit vector relative to $\mathbf{r}_i$, and k_0 is the wavenumber. The magnetic vector field on the cross-section of the 4 resonators and computed from Eq. (1) is shown in Fig. 1 for each mode. The 90° rotational symmetry of the structure implies that the modes $\left(\begin{smallmatrix}-&+\\-&+\end{smallmatrix}\right)$ and $\left(\begin{smallmatrix}+&+\\-&-\end{smallmatrix}\right)$ are degenerated, i.e., they resonate at the same frequency. In the next paragraph, we aim to use the uniformity of the magnetic field associated to the mode $\left(\begin{smallmatrix}-&+\\-&+\end{smallmatrix}\right)$ to improve the homogeneity of the magnetic field delivered by a simple loop coil.

The set-up for the numerical experiment consists of the aforementioned 4 hybridized half wavelength resonators excited by a loop coil (see the inset of Fig. 2). For all configuration (with and without the HC), the resonance frequency of the system is tuned to 300 MHz and matched to 50 Ω using a matching network circuit. The 3-cm diameter loop coil generates a magnetic field that is mainly parallel to (Oy) axis. The magnetic field generated by the loop coil alone is shown in Fig. 2(a). The magnetic field drops off quickly. Under a quasi-static assumption, the magnetic field decreases as $1/\sqrt{R^2+d^2}$, where R is the radius of the loop, and d is the distance from the loop axis. When the loop is in the near field of the four resonators, we clearly observe two strong resonances on the reflection parameter. Indeed, due to the antisymmetry plane of the system with respect to (Oyz), only the eigen-modes $\left(\begin{smallmatrix}-&+\\-&+\end{smallmatrix}\right)$ and $\left(\begin{smallmatrix}-&+\\+&-\end{smallmatrix}\right)$ can be excited. The magnetic field pattern of the first resonance in the plane (Oxy) and (Oyz) is shown in Figs. 2(c) and 2(d). We observe, as expected, that the first resonance corresponds to the magnetic mode $\left(\begin{smallmatrix}-&+\\-&+\end{smallmatrix}\right)$. The field in the region inside the 4 resonators is much more homogeneous than the one obtained with the coil loop alone in the transverse section (Oxy). Also, the field is now extended over all the resonator length in the longitudinal sections (Oyz) and (Oxz).

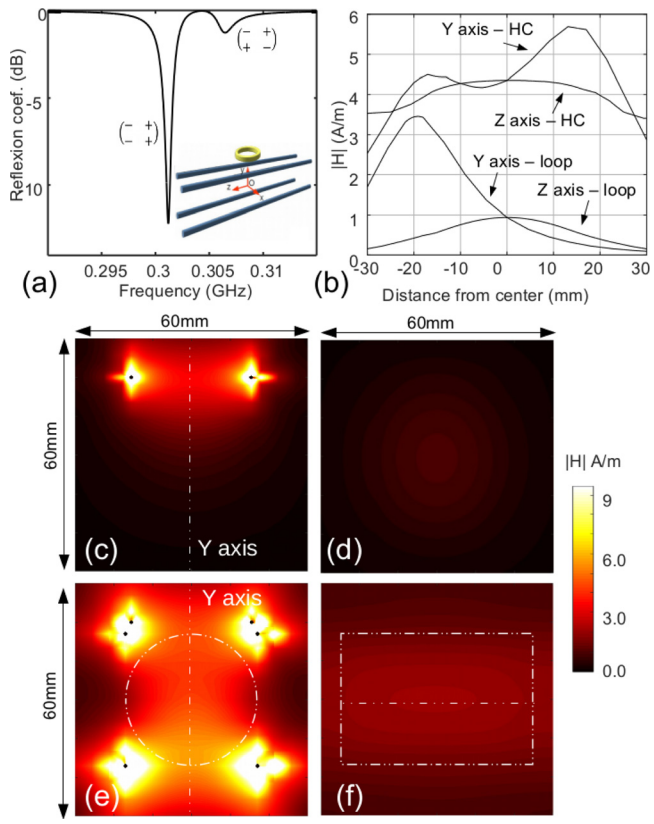

FIG. 2. (a) Simulated reflexion parameter (S_{11}) of the magnetic coil in front of the HC. Inset: schematic view of the surface loop coil and of the HC and the definition of the coordinate system. (b) Four magnetic field magnitude profiles on four axis shown in Figs. 2(c)–2(f). (c) [respectively, (e)] Magnetic field magnitude generated by the loop coil without [respectively, with] the resonators on plane (Oxy). (e) [respectively, (f)] Magnetic field magnitude generated by the loop coil without [respectively, with] the resonators on plane (Oxz).

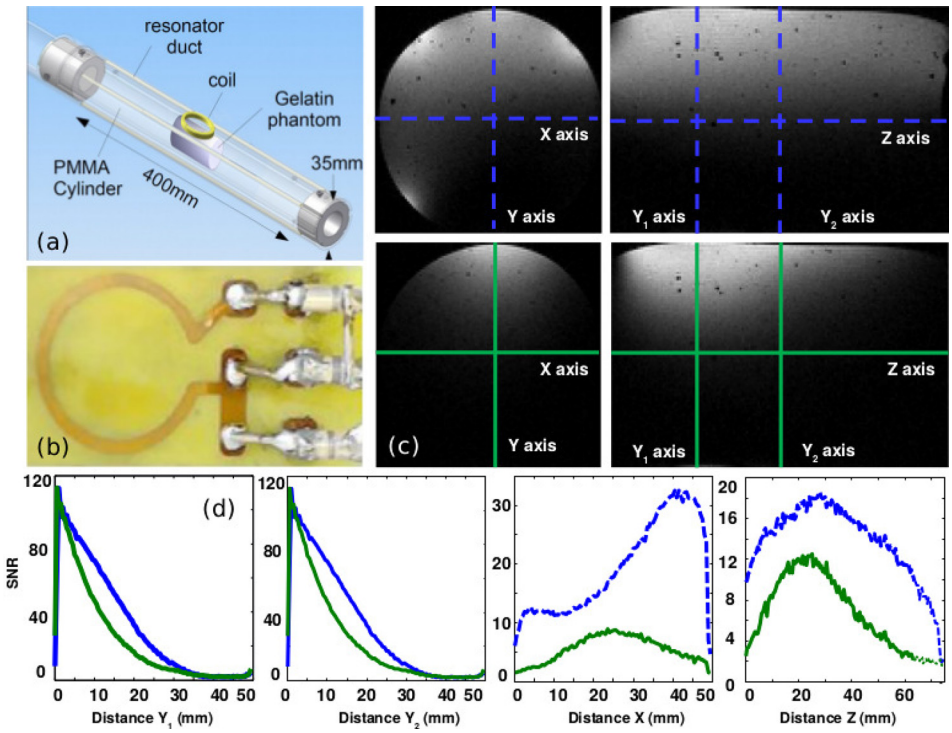

FIG. 3. (a) Experimental MRI test bed with the gelatin phantom. (b) The loop coil. (c) Sections of a cylindrical gel with (first row) and without (second row) the HC. From left to right, the transverse, sagittal planes. (d) Four SNR profiles with (dashed line) and without (continuous line) HMC. The four axes are shown in Fig. 3(c).

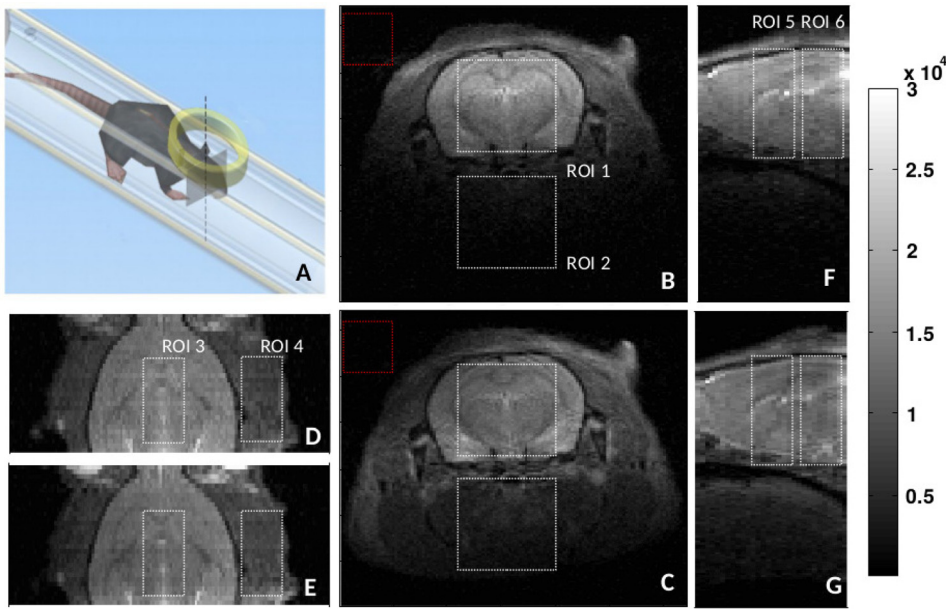

FIG. 4. (a) Schematic view of the rat inside the MRI bed, the resonators, and the loop coil. (b) *In vivo* demonstration of the sensitivity and homogeneity improvement of a single loop coil. Axial (a) and (b), coronal (c) and (d), and sagittal (e) and (f) views of a rat head from the same spin-echo acquisition at 7 T without (a), (c), and (e) and with (b), (d), and (f) hybridized rods positioned around the rat. The following settings were used for this turboRARE sequence: 128 × 128 matrix size, 30 slices with voxel size of 275 μm × 235 μm × 500 μm, RARE factor = 8, TE/TR = 24 ms/3000 ms, NA = 8. The position of the various 3D regions of interest used to calculate mean signals is drawn as white dashed rectangles. The region of interest used to calculate the standard deviation of the noise is the red dashed square.

Experimental validations of HC are performed in a 7 T small animal MRI scanner (Pharmascan, Bruker Biospin, Germany) equipped with 300 mT/m gradient coils. The HC is used in transmit-receive mode. The hybridized coil is made out of thin metallic rods and tubes, composed of non-ferrous materials: pure copper. Four resonators are attached inside a PMMA cylinder to form a right parallelepiped (see Fig. 3(a)). The length of the rods is roughly 375 mm

TABLE I. Comparison of SNR with and without HC obtained on 6 ROI.

	In depth		Lateral		Longit.	
ROI#	1	2	3	4	5	6
SNR w/o HC	33.2	4.2	30.8	14.4	31.6	27.7
SNR w/ HC	31.7	10.2	30.2	18.7	31.0	27.1

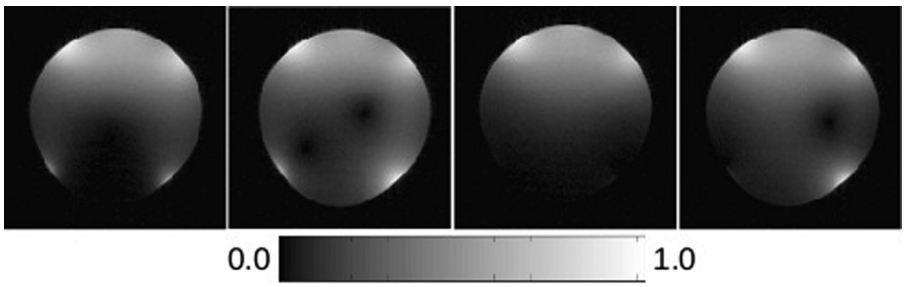

FIG. 5. Four MR axial images obtained on the gel phantom for four different combinations of resonance frequency of the four resonators.

because the Larmor frequency of proton at 7 T equals 300 MHz. When the dielectric material under study is included between the four resonators, the resonance frequencies of the hybridized modes are slightly modified. To mitigate this effect, the length of the resonators can be adjusted. To that end, each resonator is made of a copper rod which can slip into a copper tube. This allows a fine-tuning of their resonance frequency. The side length of the square cross section is 35 mm. The MRI acquisitions were done using a 30 mm-diameter copper surface coil etched on a 1 mm-thick dielectric substrate. Even if the loop matching is much better when coupled to the 4 resonators (see Fig. 2), it is not yet sufficient for a MRI application. To reach efficiency close to 100%, we use a classical matching network made of tunable amagnetic capacitors to match perfectly for every acquisition. First, HC concept is validated with a homogeneous phantom. The lastest is a cylinder made of gelatin whose diameter and length are equal to 50 mm and 110 mm, respectively. The phantom is placed between the four half-wavelength resonators.

Fig. 3(b) presents MRI images of axial, sagittal, and coronal planes of the gel obtained with and without the hybridized resonators. The MRI sequence used to obtain these image is a fast T_1-weighted 2D gradient echo sequence (isotropic resolution 0.5 mm, matrix size $100 \times 100 \times 150$, TE = 3.8 ms, TR = 1321 ms, and flip angle 50°). The air bubbles inside the gel generate black dots in the image. We observe that the hybridized mode provides images that are much more homogeneous and extended than the one obtained with the loop alone. However, we observe that coupling with one resonator at the bottom is not as good as predicted by theory. This is because the gel partially shields the electrical field which is the main origin of coupling. Moreover, due to the complex environment of an MRI cavity, the coupling of the 4 resonators is harder to obtain. Note that we did not observe any susceptibility artifacts. They only occur in the very close vicinity of the 4 resonators. Fig. 3(d) shows SNR along several axes through the gel. The *in vitro* SNR profiles were calculated as follows:[15] First, the signal was averaged over a 6×6 voxels at each position. Second, the signal to noise ratios were obtained by dividing this signal by the standard deviation of the signal measured in a $15 \times 10 \times 150$ voxel box located in a region where no signal is expected (outside the gel). We observe a significant enhancement of the SNR in all the volume of HC.

Finally, the HC has been validated *in vivo* by imaging the head of a rat. The operation is performed under general anesthesia. The rat is placed on a bed support inside the PPMA cylinder. The head is located in the center of the HC (see Fig. 4(a)). Fig. 4 shows the 3 projections of a 3D T2 spin-echo acquisition. During the same experiment, this is compared with the metallic rods removed from the PPMA cylinder and the loop coil retuned and rematched (Fig. 4(b)). We clearly observe that HC allows a deeper visualization of the head. Finally, the image is much more uniform with HC. To quantify this observation, we report on Table I, *in vivo* SNR values obtained by dividing the signal averaged in the various ROI (Region Of Interest) plotted in Fig. 4 by the standard deviation of noise measured outside the head. The strong increase of the SNR in depth gives access to much more anatomic details. No degradation and even improvements are observed in the two other directions.

The system composed of the 4 resonators and the loop coil can be interpreted as a volumetric coil because the object under test lies between the resonators. One of the closest system routinely clinically used is the bird cage.[3] Here, the resonance frequencies are now fixed by the resonance frequency of the half-wavelength dipoles and the hybridization effect. The conception of the HC is very simple because it does not require any MRI compliant passive elements and can be used with a simple external coil. The straight hybridized rods are not interconnected with each other and not connected to the active loop coil. That makes the design easier. The counterpart is a resonance frequency more sensitive to the dielectric index of the object under study. Moreover, because each dipole is an electric resonator, the system under study will be exposed to RF electrical field that can induce heat.

Finally, we show how by modifying independently each resonator length, i.e., their fundamental frequency, the B1 pattern is modified. In Fig. 5 are plotted 4 images of the same gelatin phantom using the HC with half-wavelength tunable resonators. This property provides a degree of freedom to control and engineer the B1 field distribution.

We have proposed an original coil based on hybridization between resonators. We have demonstrated that compared to a coil, the signal to noise is increased by about 200% in the region of interest. The uniformity of the distribution of the field is improved in all directions. The set-up presents a very simple design and a high geometric adaptability. Prior to a clinical application (7 T or 3 T MRI), one should evaluate the electromagnetic compatibility of the HC.

We gratefully acknowledge the financial support of the French Government-funded technological research organization CEA/DAM. This work was supported by the French National Agency (ANR) with the Grant OPTRANS (No. 2010 BLAN 0124 04), by the LABEX WIFI (Laboratory of Excellence ANR-10-LABX-24) within the French Program Investments for the Future under reference ANR-10-IDEX-0001-02 PSL* and by the Institut Carnot STAR funding through the project CMRI.

[1]Z.-P. Liang and P. C. Lauterbur, *Principles of Magnetic Resonance Imaging* (SPIE Optical Engineering Press, 2000).
[2]S. E. Solis, R. Wang, D. Tomasi, and A. O. Rodriguez, Phys. Med. Biol. **56**, 3551 (2011).
[3]C. E. Hayes, W. A. Edelstein, J. F. Schenck, O. M. Mueller, and M. Eash, J. Magn. Res. **63**, 622 (1985).
[4]P. B. Roemer, W. A. Edelstein, C. E. Hayes, S. P. Souza, and O. Mueller, Magn. Res. Med. **16**, 192 (1990).
[5]U. Katscher and P. Börnert, NMR Biomed. **19**, 393 (2006).
[6]A. Hoyos-Idrobo, P. Weiss, A. Massire, A. Amadon, and N. Boulant, IEEE Trans. Med. Imaging **33**, 739 (2014).
[7]J. B. Pendry, D. Schurig, and D. R. Smith, Science **312**, 1780 (2006).
[8]J. M. Algarin, M. J. Freire, M. A. Lopez, M. Lapine, P. M. Jakob, V. C. Behr, and R. Marques, Appl. Phys. Lett. **98**, 014105 (2011).
[9]M. J. Freire, L. Jelinek, R. Marques, and M. Lapine, J. Magn. Res. **203**, 81 (2010).
[10]M. S. Khennouche, F. Gadot, B. Belier, and A. de Lustrac, Appl. Phys. A **109**, 1059 (2012).
[11]X. Radu, D. Garray, and C. Craeye, Metamaterials **3**, 90 (2009).
[12]A. Christ, O. J. F. Martin, Y. Ekinci, N. A. Gippius, and S. G. Tikhodeev, Nano Lett. **8**, 2171 (2008).
[13]S. J. Orfanidis, *Electromagnetic Waves and Antennas* (Rutgers University, 2014).
[14]R. Abdeddaim, A. Ourir, and J. de Rosny, Phys. Rev. B **83**, 033101 (2011).
[15]J. T. Bushberg and J. M. Boone, *The Essential Physics of Medical Imaging* (Lippincott Williams & Wilkins, 2011).